https://doi.org/10.3311/PPee.43225 | 1

Periodica Polytechnica Electrical Engineering and Computer Science

Design and Realization of Double-star Squirrel Cage Induction Motor

Abbas Sadia[1*], Roubache Lazhar[2], Ghedamsi Kaci[3], Iffouzar Koussaila[2]

[1] Laboratoire de Technologie Industrielle et de l'Information (LTII), Faculté de technologie, Université de Bejaia, 06000 Bejaia, Algeria
[2] Laboratoire de Recherche des Systèmes Electriques et de Conversion d'Energie,Département d'Electrotechnique, Ecole Nationale Supérieure des Technologies Avancées,Dergana-Bordj El Kiffan,16087 Algiers, Algeria
[3] Laboratoire de Maitrise des Energies Renouvlables,Département de génie électrique, Faculté de technologie,Université de Bejaia, 06000 Bejaia, Algeria
[*] Corresponding author, e-mail: sadia.abbas@univ-bejaia.dz

Received: 08 January 2026, Accepted: 07 July 2026, Published online: 07 September 2026

Abstract

This article presents an in-depth study and a systematic design of a double-star squirrel-cage induction motor with a rated power of 3 kW and a synchronous speed of 3000 rpm. The proposed design method is supported by a thorough finite element analysis performed using electromagnetic simulation tools. The design calculations and simulation results were validated through the fabrication and experimental testing of a prototype of the machine. The test results show excellent agreement with the theoretical predictions and numerical simulations, thereby confirming the effectiveness and accuracy of the proposed design method. In fact, the calculated stator resistance R_1 at 20°C is 13.24 Ω, while the simulated value is 13 Ω. The experimental measurement taken at 23 °C yields a resistance of 13.22 Ω. The expected rotational speed is 2880 rpm, and the simulation speed is N_r = 2940 rpm, whereas the rotor speed obtained during the experimental tests is 2931 rpm. The rated power factor cos φ = 0.84, while the value obtained experimentally is 0.82. This deviation is small and is consistent with the expected behavior of the machine.

The results obtained highlight a strong correlation between theoretical analyses, numerical simulations, and experimental tests, thereby demonstrating the suitability of the double-star squirrel-cage induction motor configuration for high-performance industrial applications.

Keywords

multiphase induction machine, experimental realization, analytical design, behavior analysis

1 Introduction

The global climate is warming due to greenhouse gas emissions, which are primarily caused by the burning of fossil fuels [1, 3, 9]. In light of this situation, the global energy landscape is undergoing a major transformation, marked by a transition toward more sustainable and environmentally friendly energy sources. Renewable energy plays a vital role in this transition, as it comes from natural resources that continually regenerate and pose a low risk of depletion in the short term [3, 4]. They offer energy solutions that are both reliable and stable. They make a significant contribution to reducing the effects of climate change. They also help reduce environmental degradation. [1–10].

Renewable energy encompasses many sources, including hydroelectric power, wind power, solar power, geothermal energy, and energy generated from biomass.

Global energy demand continues to rise. That is why it has become crucial to transition to renewable energy. This helps promote environmental sustainability and reduce greenhouse gas emissions [1]. It is therefore very important to develop electrical systems that function well and are easily adaptable, especially electric machines that can efficiently utilize renewable energy. This means that research is needed to develop innovative motors. These motors must be highly efficient, robust, and energy-efficient to meet the needs of modern energy systems that aim to protect the environment.

Wind power is now the second-largest source of renewable electricity, just behind hydropower [7–8]. In recent years, its development has accelerated significantly.

Technological advances and falling costs have been the main drivers of this growth [3–11]. A wind energy conversion system generally consists of several components that

Cite this article as: Sadia, A., Lazhar, R., Kaci, G., Koussaila, I. "Design and Realization of Double-star Squirrel Cage Induction Motor", Periodica Polytechnica Electrical Engineering and Computer Science, 2026. https://doi.org/10.3311/PPee.43225

work together to efficiently convert the kinetic energy of the wind into electrical energy. This system mainly consists of a wind turbine, a drive shaft, a rotating electric generator, and an electronic power converter that can operate in one direction or both directions. When the wind turbine rotates at a relatively slow speed, typically a few dozen revolutions per minute, a speed multiplier, also known as a gearbox, is installed between the wind turbine and the rotating electric generator. This optimizes the transfer of energy between the wind turbine and the rotating electric generator, thereby improving the overall efficiency of the wind energy conversion system [2].

There are various types of generators used in wind power conversion systems. Induction motors are increasingly being used [11]. They offer numerous advantages. Induction motors provide good power generation capacity. They are also very reliable. The performance of asynchronous machines is satisfactory. They have a simple and robust design. Furthermore, asynchronous machines have low manufacturing costs. They are therefore particularly well-suited for wind power applications [16].

The double-star squirrel-cage induction motor (DSSCIM) is a machine of great interest. It has a highly original configuration. It is equipped with two independent three-phase windings on the stator. Its rotor is similar to that of a conventional squirrel-cage induction motor. This configuration gives it great flexibility. It also improves its performance in certain applications. It is particularly useful in renewable energy generation systems.

The double-star squirrel-cage induction motor (DSSCIM) offers several significant advantages, just like other polyphase motors. It provides intrinsic power distribution and high overload capacity. In addition, it significantly reduces fluctuations in electromagnetic torque and losses in the rotor [5, 6, 12, 13, 17]. These characteristics make double-star asynchronous motors highly efficient and reliable in applications where operational stability and energy efficiency are essential. Consequently, double-star asynchronous motors are used in many fields, including embedded systems and information technology infrastructure [14–15].

In addition to applications related to renewable energy, double-star squirrel-cage induction motors are used in electric traction, marine propulsion, high-power industrial drives, aerospace systems, and energy generation and storage applications [18].

Despite its many advantages, particularly in terms of reliability, reduced torque ripple, and fault tolerance, however, to date; the double-star asynchronous motor has not yet been adopted in industrial applications and remains the subject of ongoing research and development due to its high manufacturing cost and the complexity of its control system since its design requires two sets of stator windings as well as a more sophisticated power converter, which increases the overall cost of the system.

2 Analytical design of DSSCIM

The analytical design of a double-star squirrel-cage induction machine is a multifaceted process comprising several stages intended to optimize its electromagnetic performance, energy, efficiency, and operational reliability.

2.1 Specifications of DSSCIM

An analytical approach for the study and sizing of the double-star squirrel-cage induction motor (DSSCIM) is presented below. In this configuration, the two star-connected stator windings are housed within the same stator magnetic circuit and are offset by 30° electrical from one another. Both windings have the same number of poles and operate at the same supply frequency. The prototype of this machine was manufactured by Electro-Industries, located in Azazga, in the wilaya of Tizi Ouzou, Algeria. Its main design parameters and rated characteristics are presented in Table 1.

Analytical formulations derived from the fundamental conservation laws governing mass, momentum, and energy flows within the various components of the machine enable the determination of its remaining dimensional parameters.

2.2 Geometrical design

2.2.1 Electromagnetic power

Analytical expressions derived from the fundamental laws of magnetic flux conservation in the various parts of the machine are used to calculate the remaining geometric

Table 1 Summary of the machine's specifications

Symbol	Quantity	Value	Unit
P_n	Rated power	3	kW
m_1	Phase number	6	–
$2P$	Number of poles	2	–
f_1	Frequency	50	Hz
U_n	Rated voltage	400	V
I_n	Rated Current	6.7	A
N_r	Rotational speed	2880	rpm
$\cos\Phi$	Power factor	0.84	–
Cl	Insulation class	F	–
IP	Ingress protection	54	–

parameters. Electromagnetic power [19] corresponds to the conversion of electrical energy into mechanical energy, thereby generating electromagnetic torque:

$$P_e = k_e \frac{P_n}{\eta_n \times \cos(\phi_n)}, \quad (1)$$

k_e is defined by the following equation (Eq.(2)):

$$k_e = 0.98 - 5 \times P \times 10^{-3}. \quad (2)$$

2.2.2 Virtual air-gap length

The introduction of the virtual air gap length [19] makes it possible to account for the dispersion of the magnetic field in the air gap, leading to a more accurate analytical evaluation of the machine's electromagnetic characteristics.

$$L_i = \frac{6.1 \times 10^{12} \times P_e}{\alpha_i \times K_f \times N \times D_1^2 \times A_1 \times B_\delta \times K_{en1}}. \quad (3)$$

With α_i: The virtual polar coverage coefficient amounts to 0.64, assuming sinusoidal induction; K_f: the air-gap flux-density waveform factor is equal to 1.11; D_1: the bore diameter is equal to 80.64 mm and K_{en1}: the stator winding factor is equal to 0.958.

2.2.3 Stator head thickness

The stator head thickness [19], which corresponds to the height of the stator back, is a fundamental design parameter in electrical machines, as it directly affects the magnetic flux distribution, mechanical rigidity, and heat dissipation characteristics of the stator.

$$h_{c1} = \frac{D_{ext} - D_{moy}}{2}. \quad (4)$$

2.2.4 Maximum diameter of the rotor

The rotor's maximum diameter [19] has a significant impact on the machine's electromagnetic output, mechanical stability, and thermal management. Therefore, selecting the rotor requires a careful balance between performance optimization and structural integrity.

$$D_2 = D_1 - 2\delta. \quad (5)$$

The various geometric dimensions of the stator and rotor slots, which play a significant role in determining the magnetic field distribution and overall performance of the machine, are shown in Fig.1.

2.2.5 Rotor back iron thickness

Once the magnetic flux passes through the rotor teeth, the magnetic circuit is completed via the outer portion of the rotor, commonly referred to as the rotor yoke. The height of the rotor yoke represents the radial thickness of this region and plays a critical role in preventing magnetic saturation and ensuring mechanical stiffness [19].

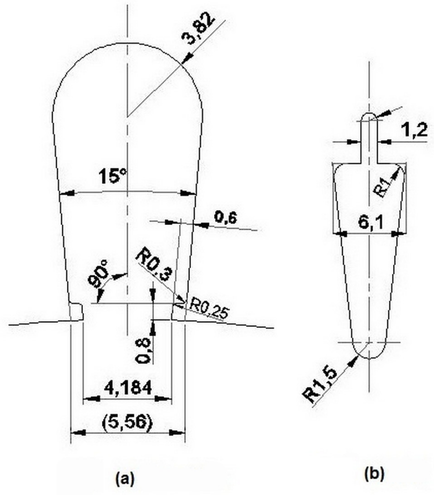

Fig. 1 Details of slots: (a) Stator slot; (b) Rotor slot

$$h_{c2} = \frac{D_2 - D_{2moy}}{2}. \quad (6)$$

3 DSSCIM winding design

Several winding configurations can be used in rotating electrical machines.

In the present design, a concentric winding scheme has been selected for both the analytical design phase and the practical implementation of the machine, due to its simplicity and ease of manufacturing.

3.1 Winding parameters

The winding configuration was designed to ensure a synchronous rotational speed of 3000 rpm, corresponding to a two-pole-pair structure ($2P = 2$). Within each star, the stator windings are evenly distributed and spatially offset by 120 electrical degrees to generate a balanced three-phase magnetic field. The coils of each phase are connected in series to achieve the target phase resistance. Furthermore, the windings are electrically insulated to prevent inter-turn short circuits and mechanically protected against thermal expansion and vibration-induced degradation.

Table 2 provides a summary of the key winding parameters, offering a clear overview of the design specifications.

3.2 Winding diagram

To improve the distribution of the magnetomotive force (MMF), a panoramic winding topology, shown in Fig. 2, has been used in the proposed design.

Table 2 Parameters of winding

Symbol	Quantity	Value	Unit
Z_1	Number of stator slots	36	–
τ_{p1}	Pole pitch	126.6	mm
t_1	Dental pitch	10.56	mm
q_1	Number of slots per pole per phase	4	–
y_1	Winding pitch	12	–

4 Electromagnetic design and parameters of the equivalent circuit

The Double Star Squirrel Cage Induction Machine (DSSCIM) investigated in this study is characterized by the presence of two identical stator stars. In this context, the electromagnetic design and the calculation of the equivalent circuit parameters are performed based on a single star, while neglecting the interactions between the two stars. This approach simplifies the analysis while maintaining the required level of accuracy, given the structural and functional symmetry of the two stars. Consequently, the results obtained for one star can be extrapolated to the entire system, thereby optimizing the design process.

The diagram shown in Fig. 3 illustrates the conventional single-phase equivalent circuit with respect to the stator of a single star of the DSSCIM.

The governing expressions for the parameters of the equivalent scheme are given as follows (Eqs. 7–11):

The stator phase active resistance [19]:

$$R_1 = \rho_{cu} \frac{W_1 \times L_{W1} \times 10^3}{a_1 \times S_{norm1}} . \quad (7)$$

Where W_1 denotes the number of turns of a parallel path; L_{W1} mean turn length and standardized cross-section of a conductor.

The total reactance [19]:

$$X_1 = \frac{1.58 \times f_1 \times L_i \times W_1^2 \times \lambda_1}{P \times q_1 \times 10^8} , \quad (8)$$

given that λ_1 represents the stator permeance.

The magnetization reactance [19]:

$$X_m = \frac{K_e \times U_{n1}}{I_\mu} . \quad (9)$$

The magnetization resistance [19]:

$$R_m = \frac{X_m \times I_\mu}{I_{0a}} , \quad (10)$$

where I_{0a} denotes the no-load current.

The rotor phase resistance relative to the stator [19]:

$$R_{2ram} = M \times R_2 . \quad (11)$$

The rotor reactance relative to the stator [19]:

$$X_{2ram} = M \times X_2 . \quad (12)$$

With:

$$M = \left(\frac{4m_1}{Z_2}\right)\left(\frac{W_1 K_{en1}}{K_{0b}}\right)^2 , \quad (13)$$

K_{0b} is the rotor slot skew factor.

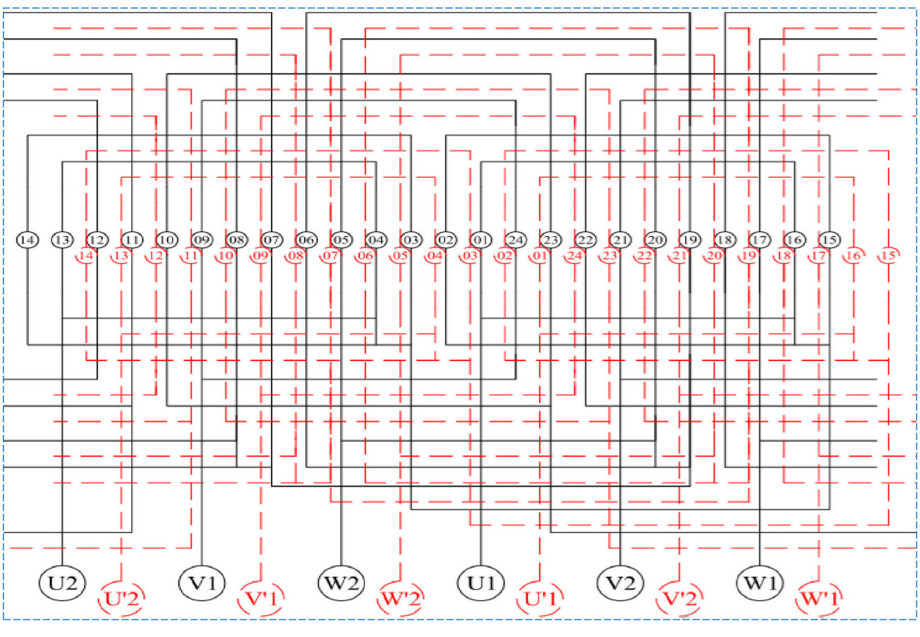

Fig. 2 Panoramic presentation of the DSSCIM winding

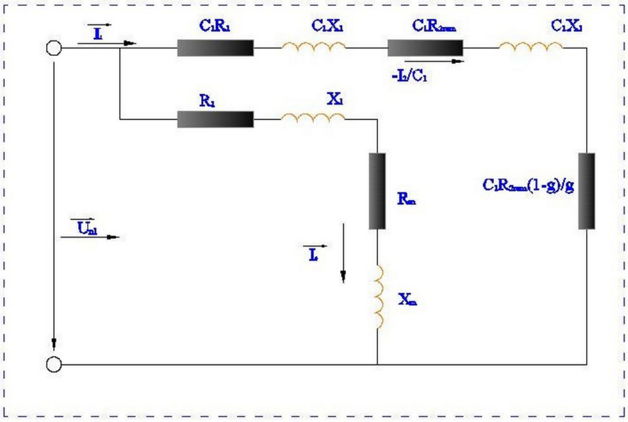

Fig. 3 Equivalent circuit diagram referred to the stator

Table 3 presents the parameter values corresponding to the equivalent circuit model of the DSSCIM.

The magnetic flux generated at a pole and the electromagnetic torque produced as follows as Eq. (14) and Eq. (15) [19]:

$$\Phi = \frac{K_e \times U_{n1}}{4 \times K_f \times W_1 \times f_1 \times K_{en1}}, \tag{14}$$

$$C_e = \frac{60 \times P_e}{g \times 2 \times \pi \times N_s}. \tag{15}$$

5 Transient finite element simulation of the designed DSSCIM

A numerical simulation was performed using ANSYS to validate the developed design. This computational approach allows for an in-depth assessment of the model's behavior by taking into account relevant physical and mechanical constraints. The implementation of this method ensures a thorough and accurate evaluation, enhancing both the optimization and reliability of the final design.

In the simulated model, two three-phase power sources with a phase shift of 30 electrical degrees are used to supply the system.

Table 3 Equivalent circuit parameters

Symbol	Value	Unit
R_1	13.24	Ω
X_1	11.12	Ω
X_m	119.50	Ω
R_m	1659	Ω
R_{2ram}	3.33	Ω
X_{2ram}	9.02	Ω

5.1 Results and discussion of transient finite element simulation of the designed DSSCIM

The simulation results correspond to operating conditions defined by a slip of s = 0.02, a rotor speed of 2940 rpm, and an effective phase voltage of 400 V. The stator resistance is 13 Ω. The rotor bars are composed of aluminum, and the stator windings are made of copper. The rotor and stator cores are modeled as iron materials with a relative permeability of μr = 4000. For simplification, iron losses and magnetic saturation effects are neglected.

The induced voltages and currents in the six phases of the DSSCIM (Double Star Squirrel Cage Induction Machine) are determined based on finite element simulation results. The temporal variations of these electrical quantities are illustrated graphically in Figs. 4, 5, and 6, which show the

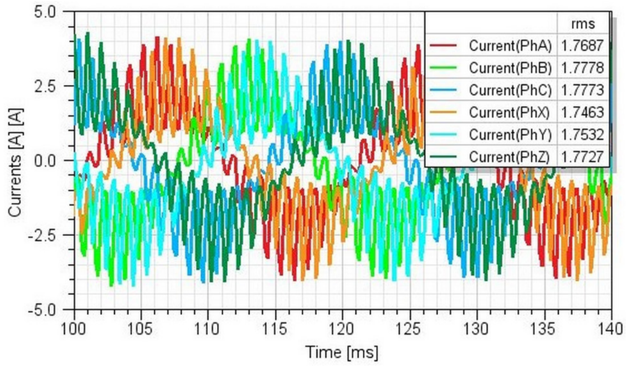

Fig. 4 Stator current

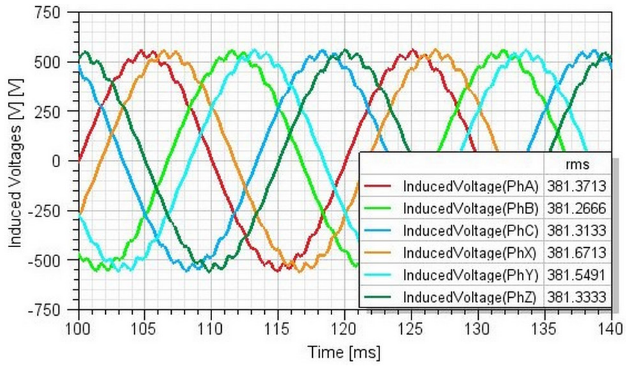

Fig. 5 Induced voltages

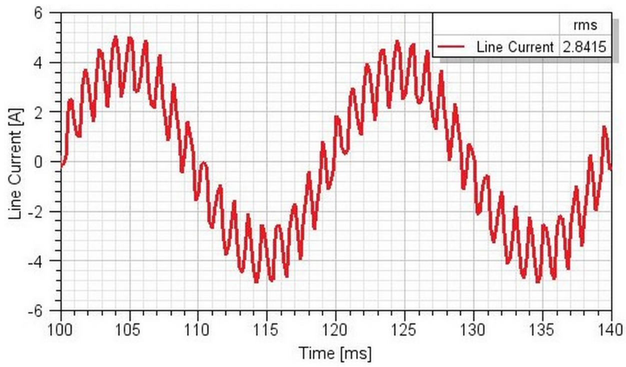

Fig. 6 Line current-time

current and induced voltage waveforms as functions of time. This method provides a comprehensive understanding of the machine's dynamic performance and electromagnetic interactions.

A finite element simulation of the double-star squirrel-cage induction motor (DSSCIM) was performed to study the spatial distribution of magnetic flux density per unit length in the various regions of the motor, as well as the corresponding current density, as shown in Fig. 7. This approach allows for an in-depth evaluation of the machine's electromagnetic behavior and its overall performance.

The spatial variation of magnetic flux density within the machine, analyzed along both the radial and tangential directions, is presented in detail in Figs. 8 and 9. These figures illustrate the distribution characteristics of the magnetic field, providing an in-depth examination of its behavior in the respective directions.

The performance characteristics of the machine, including output power, electromagnetic torque, and electrical power, are evaluated based on the developed design. These parameters are simulated and analyzed, and are illustrated graphically in Figs. 10 and 11. The resulting performance metrics are influenced by multiple design and material factors, such as the geometry of the stator and rotor, the structural configuration

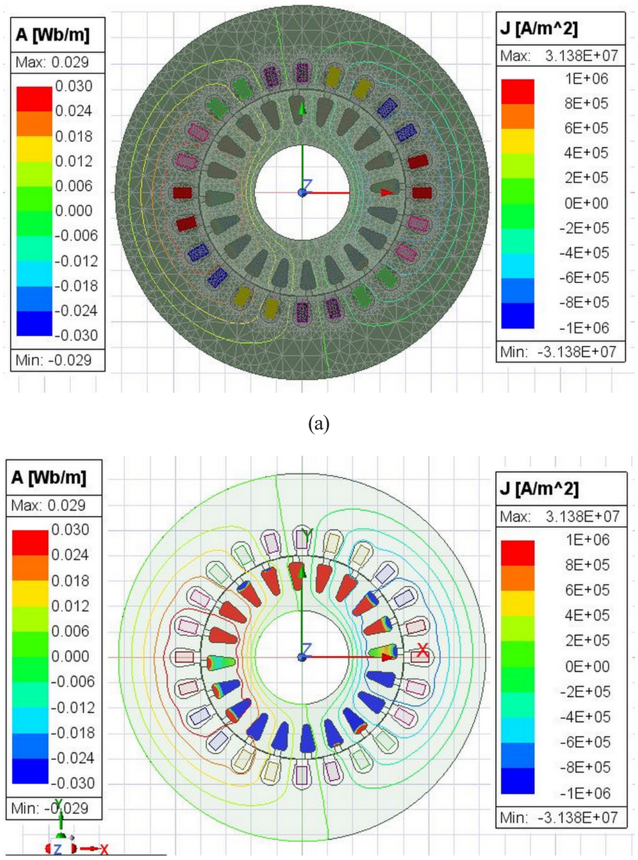

(a)

(b)

Fig. 7 Magnetic flux and current density: (a) With mesh; (b) Without mesh

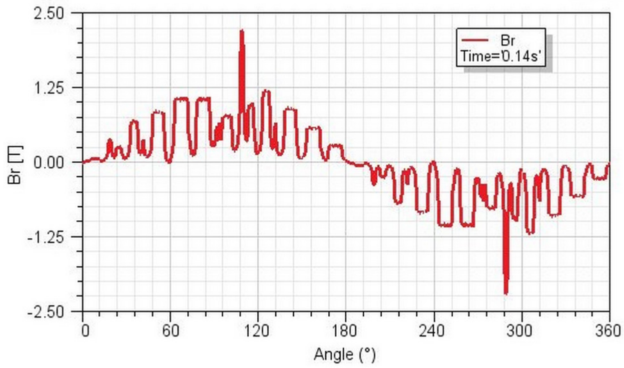

Fig. 8 Magnetic Induction in radial direction

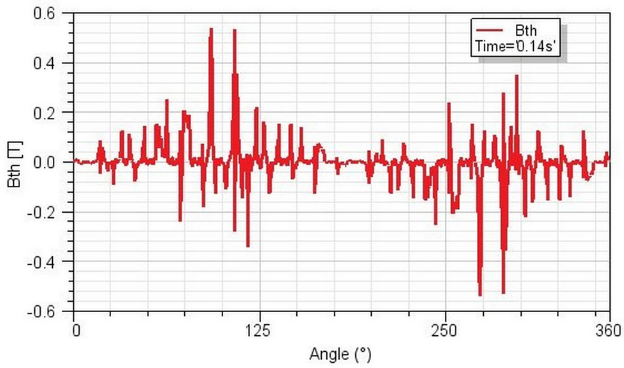

Fig. 9 Magnetic Induction in tangential direction

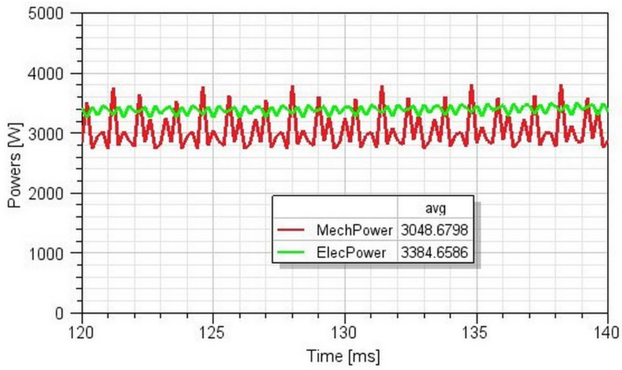

Fig. 10 Mechanic powers

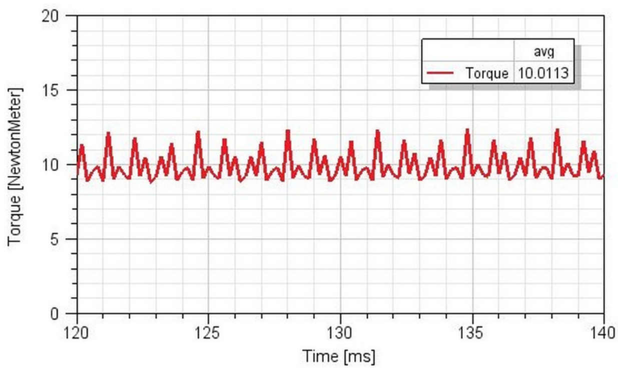

Fig. 11 Electromagnetic torque

of their cores, the winding arrangements, and the electromagnetic properties of the materials used.

6 Realization process of DSSCIM

Similar to conventional machine manufacturing processes, the production of the DSSCIM begins with the selection of raw materials and proceeds through several fabrication stages until the final product is achieved.

The design of the proposed machine complies with the recommendations specified in the relevant international standards, including IEC 60034, IEC 60072-1, and IEC 60038.

The stator and rotor magnetic circuits were constructed sequentially by stacking laminated steel sheets, as shown in Fig. 12. This fabrication technique enhances the machine's magnetic performance while significantly reducing eddy current losses. The use of laminated cores is a well-established approach in electrical machine design, aimed at improving overall efficiency and operational performance. Furthermore, this construction method ensures a uniform distribution of magnetic flux and helps mitigate mechanical vibrations and acoustic noise during operation.

The winding design was successfully completed in accordance with the defined technical specifications. This critical stage of the development process was carried out with strict adherence to precision and quality standards to ensure optimal performance of the DSSCIM. The integration of the winding into the stator magnetic circuit was carried out meticulously, reflecting careful attention to detail and ensuring the reliability of the machine. This accomplishment represents a significant milestone in the project's progress and lays the foundation for subsequent phases of analysis and validation, as illustrated in Fig. 13.

7 Experimental tests on realized machine

Once the machine had been manufactured in accordance with the proposed design, it was assembled, followed by the setup of the experimental configuration for conducting the tests, as illustrated in Fig. 14.

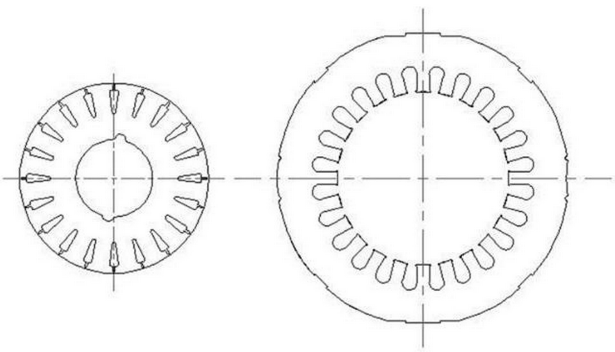

Fig. 12 Stator and rotor laminations

(a)

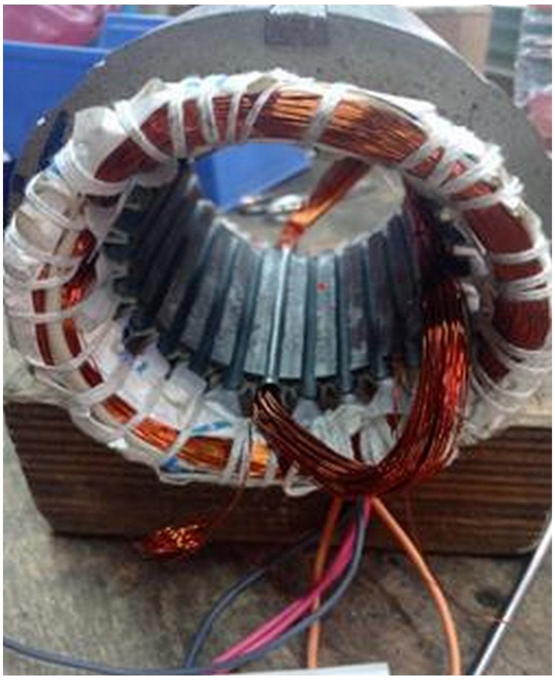

(b)

Fig. 13 Stator winding: (a) First star winding; (b) Second star winding

A series of experimental tests was then conducted on a single-engine star. All of these tests were carried out at Electro-Industries; Azazga, wilaya of Tizi Ouzou; Algeria.

The experimental setups used are described in the various tests listed below.

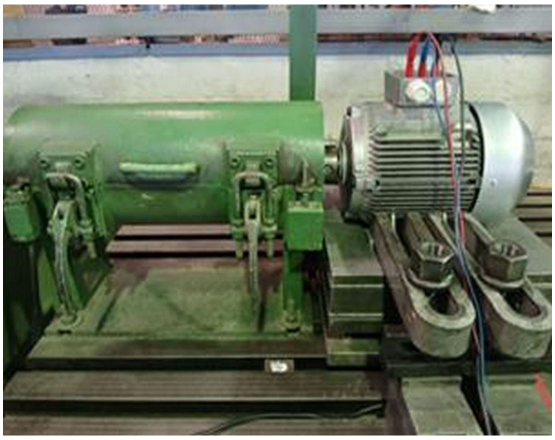

Fig. 14 Experimental setups

7.1 No-load test

The experimental setup consists of a three-phase voltage source, a wattmeter, and individual ammeters and voltmeters for each phase to directly measure the currents and voltages of the DSSCIM. To improve the accuracy of the acquired data, precision-grade ammeters and voltmeters were used throughout the measurement process.

7.2 Short-circuit test

In addition to the no-load experimental setup, a mechanical locking device was used to immobilize the rotor, thereby enabling the short-circuit test to be conducted under controlled conditions.

7.3 Thermal test

The test bench configured for the no-load experiment was retained for the thermal test. The DSSCIM was then mechanically coupled to a dynamo-brake serving as the load, to which a controlled resistive torque was applied to evaluate the machine's performance under load conditions.

A consolidated summary of the experimental results is provided in Table 4.

Table 4 Experimental results

Symbol	Quantity	Value	Unit
R_1	Stator resistance at 23°C	13.22	Ω
P_0	No-load power	0.36	kW
I_0	No-load current	2.21	A
P_{cc}	Short-circuit power	0.19	kW
U_{cc}	Short circuit voltage	55	V
I_n	Absorbed current	3.69	A
N_r	Rotational speed	2931	rpm
cosΦ	Power factor	0.82	–

8 Conclusions

This paper presents a comprehensive analysis and implementation of a double-star squirrel-cage induction machine (DSSCIM), featuring two identical stator windings offset by an electrical angle of 30°. The machine parameters were evaluated using Ansys, enabling a detailed examination of its electromagnetic behavior. The modeling and simulation results pertaining to the machine's performance were subsequently validated through experimental measurements. The close agreement between simulated and experimental data confirms the effectiveness of the computational methodology and design approach adopted. Minor deviations were nevertheless observed, largely associated with the experimental procedure, particularly the independent characterization of each stator winding. Although limited in magnitude, these discrepancies underscore the importance of adopting an integrated characterization strategy when analyzing complex electromechanical systems such as the DSSCIM.

Several avenues for future work can be identified, particularly with regard to controlling the machine under both nominal and degraded operating conditions. Greater emphasis may be placed on improving the machine's operational characteristics, with the goal of reducing energy consumption and minimizing structural mass—factors that are especially critical in embedded applications where efficiency and compactness are paramount. In addition, the detection and management of open-phase faults remain key challenges that warrant comprehensive investigation, as effective fault-handling strategies offer a promising path toward improving the robustness and reliability of advanced electrical drive systems.

References

[1] Amaka, C., Ndubuisi, O. G., Sony E. A., Ugah, T. A., Omatseyione, N., Agbakhamen, C. O., Gumi, S. A. "Advanced Renewable Energy and Sustainability: The Transitioning to Renewable Energy in Realizing Sustainable Global Energy Security", International Journal of Innovative Food, Nutrition & Sustainable Agriculture, 13(1), pp. 67–79, 2025.
https://doi.org/10.5281/ZENODO.15089182

[2] Poza Lobo, F. J. "Modélisation, Conception et Commande d'une Machine Asynchrone sans Balais Doublement Alimentée pour la Génération à Vitesse Variable" (Modeling, Design, and Control of Doubly Fed Brushless Asynchronous Machine for Variable-Speed Generation), [online] Phd thesis, Institut National Polytechnique de Grenoble, 2003. Available at: https://theses.hal.science/tel-00385804 [Accessed: 15 September 2025] (in French)

[3] Ang, T. Z., Salem, M., Kamarol, M., Das, S.H., Nazari, M. A., Prabaharan, N. "A comprehensive study of renewable energy sources: Classifications, challenges and suggestions", Energy Strategy Reviews, 43, 100939, 2022.
https://doi.org/10.1016/j.esr.2022.100939

[4] Yuan, J., Yang, R., Fu, Q. "Aspects of renewable energy influenced by natural resources: How do the stock market and technology play a role?", Resources Policy, 85, 103820, 2023.
https://doi.org/10.1016/j.resourpol.2023.103820

[5] Brahami, S, Ghedamsi, K., Achour, A., Hamoudi, Y. "Robust Model Predictive Current Control for Dual-Star Induction Machine", Periodica Polytechnica Electrical Engineering and Computer Science, 69(3), pp. 251–267, 2025.
https://doi.org/10.3311/PPee.40127

[6] Moati, Y., Kouzi, K. "Investigating the Performances of Direct Torque and Flux Control for Dual Stator Induction Motor with Direct and Indirect Matrix Converter", Periodica Polytechnica Electrical Engineering and Computer Science, 64(1), pp. 97–105, 2019.
https://doi.org/10.3311/PPee.14977

[7] Kabir, M., Sree, B. N., Khatod, K. J., Katekar,V. P., Deshmukh, S. S. "Chapter 6 - Wind energy and its link to sustainability in developing countries", In: Renewable Energy and Sustainability, Elsevier, 2022, pp. 135–178. ISBN9780323886680
https://doi.org/10.1016/B978-0-323-88668-0.00008-5

[8] Itouchene, H., Boudries, Z., Amrane, F. "Improved Power Control Based Variable Speed Wind-Turbine DFIG under Hard Work Conditions: Application of Sliding Mode Theory", Periodica Polytechnica Electrical Engineering and Computer Science, 68(4), pp. 392–412, 2024.
https://doi.org/10.3311/PPee.36760

[9] Liu., C., Liu, T. "Fossil Fuel, Greenhouse Gas and Global Warming", Global Journal of Science Frontier Research, 23(H4), pp. 21–29, 2023.
https://doi.org/10.34257/GJSFRHVOL23IS4PG21

[10] Farghali, M., Osman, A. I., Chen, Z., Abdelhaleem, A., Ihara, I., Mohamed, I. M. A., Yap, P. S., Rooney, D. W. "Social, environmental, and economic consequences of integrating renewable energies in the electricity sector: a review", Environmental Chemistry Letters, 21(3), pp. 1381–1418, 2023.
https://doi.org/10.1007/s10311-023-01587-1

[11] Abarzadeh, M., Madadi, H. K., Chang, L. "Small Scale Wind Energy Conversion Systems", In: Wind Turbines, InTech, 2011, pp. 639–652.
https://doi.org/10.5772/15937

[12] Iffouzar, K., Benkhoris, M. F., Amrouche, B., Houari, A., Ghedamsi, K., Djerioui, A. "A New Post-Fault Reconfiguration Strategy under Open-Phase Operation Conditions of Asymmetrical Double-Star Induction Machines", Energies, 16(15), 5740, 2023.
https://doi.org/10.3390/en16155740

[13] Iffouzar, K., Roubache, L., Benachour, A. "Investigation and Analysis of Electrical Faults in the Seven-phase Induction Machine", Periodica Polytechnica Electrical Engineering and Computer Science, 69(4), pp. 379–385, 2025.
https://doi.org/10.3311/PPee.40618

[14] Iffouzar, K., Damak, T. "Field-Oriented Control of Dual-Star Induction Machine with Energy Quality Based on fuzzy Logic", Revue Roumaine des Sciences Techniques Série Electrotechnique et Energétique, 70(4), pp. 483–488, 2025.
https://doi.org/10.59277/rrst-ee.2025.4.9

[15] Barrera-Llanga, K., Sapena-Bañó, A., Martínez-Román, J., Puche-Panadero, R. "Implementing Deep Learning Models in Embedded Systems for Diagnosis Induction Machine", International Journal of Electrical and Computer Engineering Research, 3(1), pp. 7–12, 2023.
https://doi.org/10.53375/ijecer.2023.319

[16] Bekbolat, S. B., Aliya, S. B., Sholpan, E. Z., Nazira, S. O., Galiya, S. I., Akmaral, A. A., Laura, S. B., Sagdat, S. S., Gulnara, B. I. "Asynchronous Motor - Operating Principle and Device", Theoretical & Applied Science, 60(4), pp. 285–289, 2018.
https://doi.org/10.15863/TAS.2018.04.60.51

[17] Gregor, R., Barrero, F., Toral, S., Durán, M. J. "Realization of an Asynchronous Six-Phase Induction Motor Drive Test-Rig", Renewable Energy & Power Quality Journal, 6(1), pp. 101–105, 2008.
https://doi.org/10.24084/repqj06.230

[18] Nounou, K., Charpentier, J. F., Marouani, K., Benbouzid, M., Kheloui, A. "Fault-Tolerant Control of VSI Driven Double Star Induction Machine for Electric Naval Propulsion", In: 2018 IEEE International Power Electronics and Application Conference and Exposition (PEAC), Shenzhen, China, 2018, pp. 1–6. ISBN 978-1-5386-6055-3
https://doi.org/10.1109/PEAC.2018.8590291

[19] Sergeev, P. S., Vinogradov, N. V., Goriainov, F. A. "Проектирование электрических машин" (Design of Electrical Machines), Energiya, 1969. (in Russian)